Received: 26 June 2019 | Revised: 27 September 2019 | Accepted: 3 October 2019

DOI: 10.1111/ejn.14600

RESEARCH REPORT

EJN European Journal of Neuroscience FENS WILEY

Modified synaptic dynamics predict neural activity patterns in an auditory field within the frontal cortex

Luciana López-Jury | **Adrian Mannel** | **Francisco García-Rosales** | **Julio C. Hechavarria**

Institut für Zellbiologie und Neurowissenschaft, Goethe-Universität, Frankfurt/Main, Germany

Correspondence
Luciana López-Jury and Julio C. Hechavarria, Institut für Zellbiologie und Neurowissenschaft, Goethe-Universität, Max-von-Laue-Straße 13, 60438 Frankfurt/Main, Germany.
Emails: LopezJury@bio.uni-frankfurt.de (LL-J); Hechavarria@bio.uni-frankfurt.de (JCH)

Funding information
Deutsche Forschungsgemeinschaft, Grant/Award Number: 275755787

The peer review history for this article is available at https://publons.com/publon/10.1111/EJN.14600

[Correction added on 20 March 2020, after first online publication: URL for peer review history has been corrected.]

Abstract

Frontal areas of the mammalian cortex are thought to be important for cognitive control and complex behaviour. These areas have been studied mostly in humans, non-human primates and rodents. In this article, we present a quantitative characterization of response properties of a frontal auditory area responsive to sound in the brain of *Carollia perspicillata*, the frontal auditory field (FAF). Bats are highly vocal animals, and they constitute an important experimental model for studying the auditory system. We combined electrophysiology experiments and computational simulations to compare the response properties of auditory neurons found in the bat FAF and auditory cortex (AC) to simple sounds (pure tones). Anatomical studies have shown that the latter provides feedforward inputs to the former. Our results show that bat FAF neurons are responsive to sounds, and however, when compared to AC neurons, they presented sparser, less precise spiking and longer-lasting responses. Based on the results of an integrate-and-fire neuronal model, we suggest that slow, subthreshold, synaptic dynamics can account for the activity pattern of neurons in the FAF. These properties reflect the general function of the frontal cortex and likely result from its connections with multiple brain regions, including cortico-cortical projections from the AC to the FAF.

KEYWORDS

auditory cortex, bats, integrate-and-fire, prefrontal cortex, sound coding

1 | INTRODUCTION

The prefrontal cortex is a clearly demarcated region within the frontal lobe of the primate brain (Goldman-Rakic, 1995). Classically, this area is known to play a critical role in the representation and execution of goal-directed behaviours (Fuster, 2001). Neurophysiological studies confirm its role in working memory, planning and decision-making (Plakke, Ng, & Poremba, 2013; Plakke & Romanski, 2014).

Several areas of the frontal cortex in primates have been shown to receive afferents from auditory processing regions

Abbreviations: AC, auditory cortex; AI, primary auditory cortex; AII, secondary auditory cortex; BF, best frequency; DP, dorsoposterior field; FAF, frontal auditory field; HF, high-frequency field; HWHH, half-width half-height; ISI, inter-spike interval; PSTH, poststimulus time histograms; sPSTH, smooth PSTH; TR, tuning ratio.

Edited by John Foxe.

(Hackett, Stepniewska, & Kaas, 1999; Romanski, Bates, & Goldman-Rakic, 1999; Romanski, Tian, et al., 1999), and some of these areas also project back to auditory centres within the forebrain as well as the midbrain of mammals (Ito et al., 2019). Accordingly, studies have shown that many prefrontal neurons are responsive to acoustic stimuli (Azuma & Suzuki, 1984; Newman & Lindsley, 1976). In addition to coding sensory stimuli, the prefrontal cortex is commonly regarded as a key area facilitating cortical audio-motor integration (Fuster, 2000). Thus, this area is involved not only in auditory cognition, multi-sensory integration (Rao, Rainer, & Miller, 1997; Watanabe, 1992) and auditory attention, but also in cognitive control of the (vocal) motor system (Carmichael & Price, 1995).

Studies on non-primate animal models have postulated that prefrontal areas (as a functional block) are not unique to primates, although this idea continues to be controversial (Uylings, Groenewegen, & Kolb, 2003; Wise, 2008). In bats, a highly used animal model for auditory studies, a frontal area responsive to sounds has also been described (Eiermann & Esser, 2000; Kanwal, Gordon, Peng, & Heinz-Esser, 2000). This area was defined as the "frontal auditory field" (FAF). Due to their nocturnal habits and their ability to echolocate, bats rely strongly on the integration of complex auditory stimuli and on the motor coordination in relation to these sensory inputs, both in echolocation and in communication contexts. It has been hypothesized that, much like prefrontal areas of primates, the bat FAF could be instrumental for the integration of sensory and motor information (Esser, 2003; Kanwal & Rauschecker, 2007; Kobler, Isbey, & Casseday, 1987). The FAF in the mustached bat (*Pteronotus parnellii*) brain receives input from at least two distinct auditory pathways, a slower pathway from the auditory cortex (AC) and a fast pathway, which bypasses the inferior colliculus and projects directly from the medulla to the frontal cortex via the suprageniculate nucleus (Casseday, Kobler, Isbey, & Covey, 1989; Kobler et al., 1987). Another route of information input is through the amygdala (Swanson & Petrovich, 1998). These afferent patterns hint towards the bat FAF as being a part of the prefrontal cortex described in other mammalian species (Goldman-Rakic & Porrino, 1985; Kobler et al., 1987), pointing to a possible executive role in decision-making and in integrating multiple time-varying inputs over time. In response to auditory stimuli, previous studies have shown longer response durations and more diverse peak response latencies in FAF neurons than in AC neurons (Eiermann & Esser, 2000; Kanwal et al., 2000). One could speculate that the multiple time-varying inputs arriving to the frontal cortex could result in different physiological properties in the FAF and AC. For example, the long FAF latencies observed in previous studies suggest that fast suprageniculate inputs alone are not sufficient for evoking FAF spiking. The latter could be either because the inputs are excitatory but not strong enough for causing suprathreshold depolarizations, or because they are inhibitory.

In this paper, using a combination of experimental data and neuronal modelling, we tested how synaptic dynamics contribute to the activity pattern of neurons in the bat FAF. First, we collected data from the bat AC and FAF and compared physiological properties in these two structures to assess the modifications to auditory-evoked responses in the AC-FAF circuit. In a second step, based on the physiological data collected, we built an integrate-and-fire neuronal model that was capable of reproducing FAF firing. The model showed that slow, subthreshold synaptic dynamics could contribute to the changes in activity patterns that occur as information travels through cortico-cortical projections from the AC to the FAF.

2 | METHODS

The experimental animals (five males and two females, species: *Carollia perspicillata*) were taken from a breeding colony in the Institute for Cell Biology and Neuroscience at the Goethe University in Frankfurt am Main, Germany. All experiments were conducted in accordance with the Declaration of Helsinki and local regulations in the state of Hessen (Experimental permit #FU1126, Regierungspräsidium Darmstadt).

2.1 | Surgical procedures

The bats were anaesthetized with a mixture of ketamine (100 mg/ml Ketavet; Pfizer) and xylazine hydrochloride (23.32 mg/ml Rompun; Bayer). Under deep anaesthesia, the dorsal surface of the skull was exposed with a longitudinal midline incision in the skin. The underlying muscles were retracted from the incision along the midline. A custom-made metal rod was glued to the skull using dental cement to fix the head during recordings. The animals recovered at least 1 day from surgery before participating in the experiments. On the first day of recordings, a small hole was made in the skull using a scalpel blade on the left side of the cortex in the position corresponding to either the AC or the FAF. To locate the FAF, the sulcus anterior (Figure 1a) was used as landmark following previous studies (Eiermann & Esser, 2000). To locate the AC, patterns of blood vessels and the position of the pseudocentral sulcus were used as landmarks (Esser & Eiermann, 1999; Hagemann, Esser, & Kossl, 2010). The craniotomies to expose the AC were made in the caudoventral region, spanning primary and secondary auditory cortex (AI and AII respectively), the dorsoposterior field (DP) and high-frequency fields (shaded regions in Figure 1b).

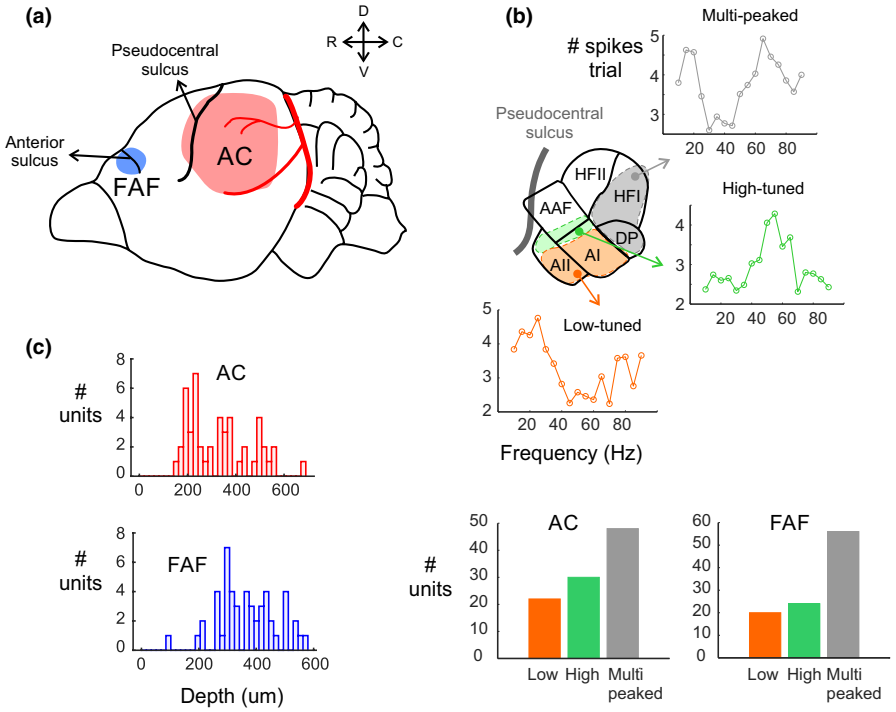

FIGURE 1 Localization of the frontal auditory field (FAF) and auditory cortex (AC) in the brain of the bat *Carollia perspicillata*. (a) Shows a sketch of *C. perspicillata*'s brain with the location of the two areas studied (modified from Eiermann & Esser, 2000). On top of (b), parcellation in the AC of *C. perspicillata*. Recordings were obtained from the tonotopic areas primary auditory cortex (AI) and secondary auditory cortex (AII) and from the most caudal high-frequency field (HFI). Three example iso-level frequency tuning curves obtained in the low-frequency portion of the tonotopic fields (low-tuned), the intersection between AI and AAF (high tuned) and the HFI field (multi-peaked) are shown. Note that the position of the dots provides only a rough estimate of anatomical coordinates within the AC based on the units' tuning curves (see also Figure S1). At the bottom of (b), percentage of AC and FAF units according to their tuning shape. Low: low-frequency tuned units (best frequency [BF] <50 kHz) with inverted V-shaped iso-level frequency tuning curves; high: high-frequency tuned units (BF ≥50 kHz) with inverted V-shaped iso-level frequency tuning curves; multi-peaked: units responding to both low and high-frequency sounds. In our dataset, low-frequency tuned units were putatively located in the caudal part of AI and AII, high-frequency tuned units derived from the rostral end of AI/AII, while multi-peaked units correspond to recordings from HFI and DP fields. (c) Depths at which responses were measured in the AC and FAF. [Colour figure can be viewed at wileyonlinelibrary.com]

2.2 | Neuronal recordings

In all seven bats, recordings were performed over a maximum of 14 days with at least 1 day recovery time between each recording session. During the experiments, the animals were always kept anaesthetized with a dose of 0.01 ml of the anaesthetic mixture used for surgery (anaesthesia was injected subcutaneously every 90–120 min). Each recording session lasted a maximum of 4 hr. The animals were positioned over a warming pad whose temperature was set to 27°C.

All experiments were performed in an electrically isolated, sound-proofed chamber. For the recordings, glass electrodes were pulled out of micropipettes (GB120F-10) with a glass puller (P-97 Flaming/Brown type micropipette puller; Sutter instruments). The electrodes were filled with a solution of potassium chloride (3 mol/L) and were attached to an electrode holder connecting the electrode with a custom-made preamplifier with 10-fold amplification through a silver wire. Electrode impedance ranged from 4 to 12 MΩ. Electrodes were moved into position within the cortex with the aid of a Piezo manipulator (PM 10/1; Science Products GmbH). The average depth of recordings in the AC was 333 μm (SD = 130) and 368 μm (SD = 102) in the FAF (Figure 1c).

Recorded electrophysiological signals were filtered between 300 and 3,000 Hz and amplified with a dual channel filter (SR 650; Stanford research). Signals were digitized with an acquisition board (DAP 840; Microstar Laboratories; sampling rate = 31.25 kHz) and stored on a computer for offline analysis.

2.3 | Acoustic stimulation

All acoustic stimuli were synthetized using a custom-written DELPHI software, generated by a D/A board (DAP 840; Microstar Laboratories; sampling rate = 278.8 kHz), attenuated (PA5; Tucker Davis Technologies) and amplified (Rotel power amplifier, RB-850). Sounds were then produced by

a calibrated speaker (ScanSpeak Revelator R2904/700ß; Avisoft Bioacoustics), which was placed 13 cm in front of the bats nose. The speaker's calibration curve was obtained with a microphone (model 4135; Brüel & Kjaer).

We used 2 ms pure tones (0.2 ms rise/fall time) to characterize auditory responses. The sound pressure level of the pure tones was set to 60 dB SPL, and their frequency changed randomly in the range from 10 to 90 kHz (5 kHz steps, 50 trials). The repetition rate for stimulus presentation was 2 Hz.

2.4 | Neuron model

To model the spiking of FAF neurons, we used a simple leaky integrate-and-fire neuron model simulated with the Brian simulator (Goodman & Brette, 2009). In the model, the membrane potential (V_m) is governed only by the subthreshold dynamic, after the following equation:

$$\frac{dV_m}{dt} = \frac{g_m\left(E_l - V_m\right) + I_s}{C_m} + \sigma\sqrt{2/\tau_i}x_i \quad (1)$$

where $g_m = 4$ nS is the leak conductance, $E_l = -50$ mV is the resting potential, $C_m = 1$ pF is the membrane capacitance, and I_s is the current from synaptic input. The neuron fires when V_m reaches the threshold $V_t = -40$ mV and then resets to $V_r = -55$ mV.

To allow for spontaneous activity, the neuron receives a random noise current added as an Ornstein–Uhlenbeck process with *SD* $\sigma = 7$ mV and time constant $\tau_i = 10$ ms, given by the last term of the Equation (1).

The equation defining the synaptic current,

$$I_s = g_e\left(E_s - V_m\right) \quad (2)$$

includes the synaptic reversal potential, $E_s = 0$ mV (standard for excitatory synapse), and the time-varying synaptic conductance, g_e, which evolves according to the differential equation

$$\frac{dg_e}{dt} = -\frac{g_e}{\tau_e} \quad (3)$$

where the time constant τ_e determines the time course of the synaptic conductance change. When a spike arrives at a synapse, the synaptic conductance changes according to

$$g_e \rightarrow g_e + w_e \quad (4)$$

where w_e is the synaptic weight, a positive value of conductance. There is an intrinsic delay in the synaptic response dominated by the membrane time constant. In addition to the delay caused by membrane properties, in the model we also included an axonal delay of 15 ms.

All the parameters were set to reproduce the extracellular activity of FAF neurons. To ensure the latter, all values used were chosen so that they encompassed the range of values described for most of the neurons studied (see Results). To study the effects of the synaptic dynamic on the spiking of FAF neurons, we performed several simulations changing two parameters: the magnitude of the synaptic weight, w_e, and the time constant of the synaptic conductance change, τ_e.

We simulated a single postsynaptic integrate-and-fire neuron, representing an FAF neuron, receiving an excitatory input through one synapse. The presynaptic spikes were generated from a Poisson process, in which the mean frequency of spike occurrence increases from 2 to 200 Hz for 25 ms after 10 ms of simulation, and then, it returns to 2 Hz until the simulation ends. Note that a one-synapse simulation is a simplified situation in which it is assumed that the feedforward input arriving to the FAF from the AC is strong enough for triggering spikes. We chose this approach because data from both the FAF and the AC obtained using identical stimulation paradigms were also available in this study. Electrophysiological data pertaining auditory responses in the *suprageniculate* nucleus (a structure that also provides input into the FAF (Casseday et al., 1989; Kobler et al., 1987)) are, to our knowledge, not available at present.

2.5 | Data and simulations analysis

To extract spike waveforms from the filtered signal, we selected a 4-ms time window around peaks whose amplitude was at least three standard deviations above the recording baseline. The waveform recorded on these time windows were sorted using a principal component analysis (PCA). For spike sorting, we used an automatic clustering algorithm, "KlustaKwik," that uses the obtained results from the PCA to create spike clusters. For each recording, we considered only the spike cluster with the highest number of spikes.

All the recording analysis was made using custom-written Matlab scripts (MATLAB R2018b; MathWorks). Simulations and their analysis were done using Python. All the analysis relative to physiological data, except for the iso-level frequency tuning curves, was done considering those trials corresponding to the best frequency (BF) response of each neuron.

The estimation of poststimulus time histograms (PSTH) from the real and simulated spike times was smoothed using a Gaussian kernel function with a bin size of 1 ms and a bandwidth of 5 ms. As a measure of the precision (duration) of the response, we calculated the half-width half-height (HWHH) of the autocorrelogram of the smooth PSTH (sPSTH) as described above. The inter-spike interval distributions were also estimated using a kernel density

estimator with a bin size of 1 ms and a bandwidth of 1 ms, in a range from 0 to 150 ms. The tuning ratio (TR) from iso-level frequency tuning curves was calculated as the maximal response (spike count) divided by the average of responses for all tested stimuli.

3 | RESULTS

3.1 | Sparse, long-lasting spiking is a fingerprint of FAF responses

The FAF receives auditory afferents from the AC (Kobler et al., 1987). In order to compare FAF and AC responses, a total of 100 units, 50 from each area, were recorded extracellularly in response to pure tones at different frequencies (from 10 to 90 kHz, 5 kHz steps; 60 dB SPL) in the short-tailed fruit bat *C. perspicillata*. To roughly determine in which areas of the AC the recordings were made, we used the shape of the frequency tuning curves as a criterion for AC field localization. Previous studies showed that non-tonotopically arranged areas show multi-peaked frequency tuning curves (Hagemann et al., 2010). In bats, multi-peaked frequency tuning curves could match the harmonic structure of echolocation signals (Kanwal, Fitzpatrick, & Suga, 1999). In contrast, neurons in tonotopically organized fields present primary-like V-shaped tuning (see example recordings in Figure S1, recordings in this figure are from a different dataset). We found both types of tuning curves (examples in Figure 1b top), indicating that we recorded AC neurons from tonotopically and non-tonotopically arranged fields. A 48% of the units recorded in the AC showed multi-peaked tuning and a 56% in the FAF (Figure 1b bottom). Recordings were made at an average depth of 333 μm in the AC and 368 μm in the FAF (Figure 1c).

Like AC neurons, FAF neurons displayed evidence of frequency tuning. Examples of frequency-response strength curves are shown in the first row of Figure 2, for an AC unit (Figure 2a) and for an FAF unit (Figure 2b). Both examples showed a preference for low-frequency sounds. The response to tones, determined from the number of spikes fired between 10 and 150 ms after stimulus onset, was maximum at 15 kHz for the exemplary AC unit and at 20 kHz for the FAF one. Figure 2c,d shows the raster plots and Figure 2e, the poststimulus time histograms (sPSTH, see Methods; smoothed used a 5 ms Gaussian kernel, 1 ms resolution), obtained for both example units at their respective BF. Simple visual inspection of the raster plots and sPSTHs already suggest the existence of very clear differences between FAF and AC responses in terms of their temporal response patterns: FAF responses to sounds are longer-lasting and less clear (in terms of number of spikes per time bin) than AC responses. Longer-lasting, broader sPSTHs rendered broader autocorrelation curves for the FAF example (Figure 2f). In the autocorrelograms, we measured the HWHH (grey horizontal line in Figure 2f) as an indicator of response duration or temporal precision, as reported in previous studies (Garcia-Rosales,

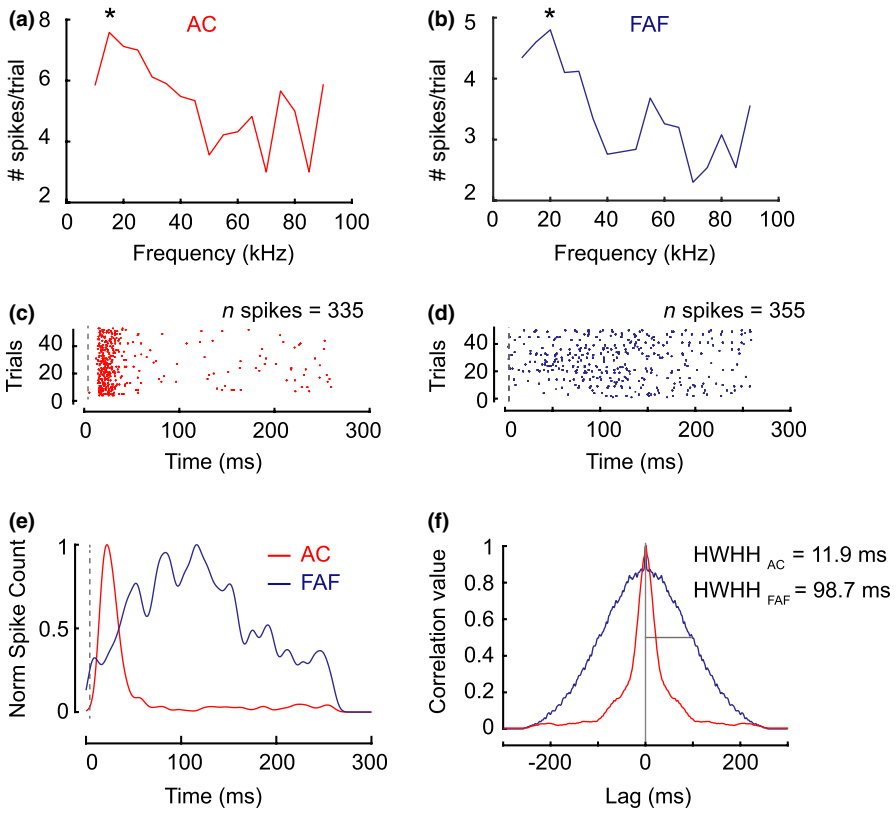

FIGURE 2 Two examples of low-frequency tuned neurons recorded from the auditory cortex (AC) and the frontal auditory field (FAF). (a) and (b) Show the number of spikes in response to pure tones at several frequencies for each unit. The number of spikes was measured as the mean of spike counts across 50 trials (from 10 and 150 ms after the pure tone onset). The asterisk indicates the best frequency (BF) and (c–f) plots correspond to the responses to these frequencies. (c) and (d) Show raster plots and (e), the corresponding smooth poststimulus time histograms (sPSTHs) for each neuron. The dashed line indicates the onset of stimulus. (f) shows the correlation values calculated from sPSTHs in the left. Grey lines represent the half-width half-height (HWHH) of the autocorrelation. [Colour figure can be viewed at wileyonlinelibrary.com]

Beetz, Cabral-Calderin, Kossl, & Hechavarria, 2018; Kayser, Logothetis, & Panzeri, 2010). The HWHH of the example FAF unit shown in Figure 2f was 98.7 ms, more than double than that of the AC unit represented in the same figure (11.9 ms).

To establish whether these differences were consistent across all recorded units, we conducted a population analysis statistically comparing each cortical area (Figure 3). There were no significant differences between the population of FAF and AC units recorded regarding their BF distributions (Kolmogorov–Smirnov test, p-value = 0.678, Figure 3a). However, the two structures did differ according to the TR of their frequency-response strength curves (Wilcoxon rank-sum test, p-value = $3.07*10^{-7}$, Figure 3b), with the AC having higher TR than the FAF. The TR is an indicator of how much the response at the BF differentiates from responses to other frequencies, and it is calculated as the spike count at the BF divided by the average of the spike count for all tested frequencies. Thus, higher TR values indicate better tuning.

Figure 3c shows the average sPSTH obtained at the BF for the units recorded in the FAF and AC. The curves were normalized to visualize the differences in the response time course

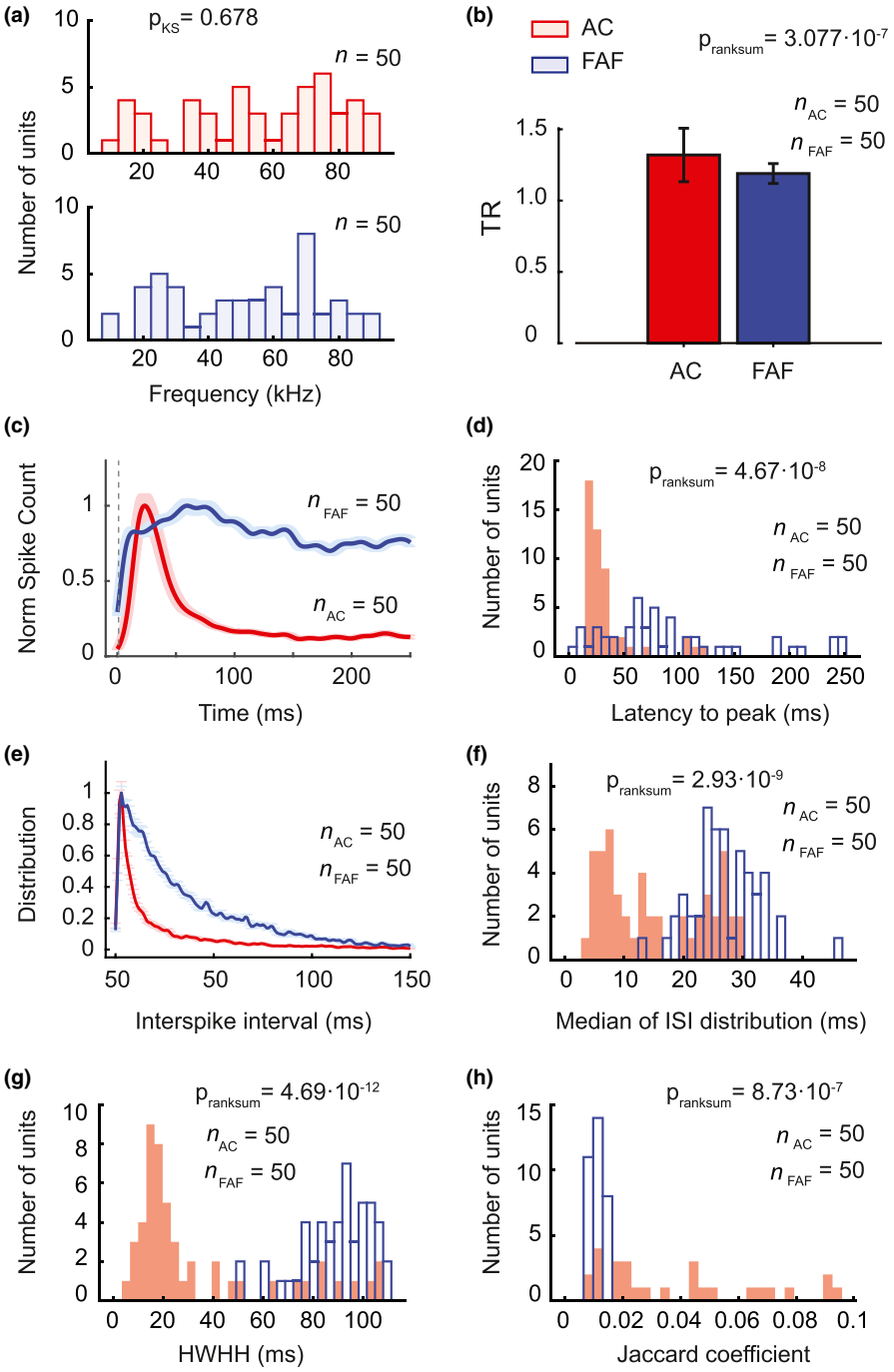

FIGURE 3 Population data comparing firing properties of 50 units recorded in the auditory cortex (AC) and 50 in the frontal auditory field (FAF). (a) Shows the distributions of best frequency (BF) obtained in the AC (top) and in FAF (bottom). (b) The mean of tuning ratio (TR) from frequency-response strength curves, calculated as spike count at BF divided by the average spike count. Error bars indicate standard deviation. All the parameters analysed in (c–h) were based on the neuronal response to the BF. (c) Shows the normalized average of smooth poststimulus time histograms (sPSTH) from all recorded units; shadow area indicates the standard error and the vertical dashed line, the onset of stimulus. (d) Distributions of peak response latencies calculated from sPSTH obtained from all units in AC and FAF. (e) Shows normalized average of ISI distribution obtained in each location: AC and FAF. (f) Distributions of median ISI for all units in AC and FAF. (g) Distributions of half-width half-height (HWHH) obtained from the autocorrelograms of sPSTHs in each location. (h) Distributions of averages of Jaccard coefficient calculated between trials as a measure of inter-trials variability, in AC and FAF. [Colour figure can be viewed at wileyonlinelibrary.com]

in the two cortical areas studied. Average sPSTHs suggest that activation in the AC precedes responses in the FAF in most of the cases. To confirm the latter, we measured peak response latencies in each neuron, calculated as the time between the onset of stimulus and the peak of the sPSTH. The distributions of peak latencies for the two cortical areas studied are shown in Figure 3d. Peak response latencies in the FAF ranged from 6 to 251 ms with an average of 93.4 ms (SD = 66). In contrast, AC units presented a narrower range of latencies with a lower average of 34.1 ms (SD = 25). The two distributions were significantly different from each other (Wilcoxon rank-sum test, p-value = $4.67*10^{-8}$). The percentage of units which present latencies lower than 20 ms was 10% in the FAF and 22% in the AC. Lower average latencies in FAF neurons have been reported in previous studies (Eiermann & Esser, 2000). Differences between our latency results and those from previous studies could be due to anaesthesia effects (ketamine–xylazine mixture [this study] versus awake, Eiermann & Esser, 2000) and/or differences in the acoustic stimuli used for triggering neuronal firing (pure tones [this study] versus FM and click stimuli, Eiermann & Esser, 2000).

To study the spike-timing patterns, we calculated the inter-spike interval (ISI) distribution in all units and plotted the normalized average distribution per cortical area (Figure 3e). The ISI distribution quantified for AC neurons was shifted to lower time intervals when compared to the FAF distribution. This result indicates that spiking in FAF neurons is slower than in the AC. The latter was also confirmed by analysing the distribution of median ISIs calculated for each unit (Figure 3f). In the FAF, the average median ISI was 26.9 ± 5.7 ms while in the AC that value amounted to 15 ± 8.7 ms and the two ISI distributions were significantly different from each other (Wilcoxon rank-sum test, p-value = $2.93*10^{-9}$).

As mentioned in the preceding text, the duration/precision of responses can be calculated by means of the HWHH obtained from autocorrelograms of the sPSTHs (in each unit, only the sPSTH at the BF was considered, see Figure 2). The histograms of HWHH obtained for the FAF and AC indicate that, in general, FAF neurons presented significantly longer response duration (and thus lower temporal precision) than AC neurons (Figure 3g, Wilcoxon rank-sum test, p-value = $4.69*10^{-12}$). The mean HWHH obtained for the FAF (88.9 ms, SD = 14.6) was more than double that observed in the AC (33.9 ms, SD = 29.1) thus indicating that temporal spiking precision deteriorates on the way to frontal areas.

In the preceding text, we mentioned that FAF neurons had irregular discharge patterns. To quantify inter-trial variability, we used the Jaccard coefficient. This metric was used in previous neurophysiological studies in bats (Macias, Hechavarria, & Kossl, 2016), and it allows to estimate the similarity between two binary words. Thus, we first transformed spike time series from each BF trial into a binary word (1 = spike, 0 = no spike, bin size = 1 ms). Next, for each pair of trials, we extracted the Jaccard coefficient and then average the results obtained across all possible trial combinations in each neuron. The values can range from 0 to 1 (1 indicates equal binary words). Figure 3h shows that the response pattern similarity across trials is statistically lower in FAF than in AC neurons (Wilcoxon rank-sum test, p-value = $8.73*10^{-7}$). The latter adds to the idea that FAF neurons present more variable discharge patterns (in this case across trials, but also within trials, see preceding text).

Several studies have found that different types of neurons can be distinguished by the duration of their action potentials (Constantinidis & Goldman-Rakic, 2002; Wilson, Scalaidhe, & Goldmanrakic, 1994). We examined whether spike widths differed between the FAF and AC to gain an insight into the spiking mechanisms in these two cortical areas. We hypothesized that the slow spiking dynamics of FAF neurons could be due to intrinsic membrane properties that could also influence spike shape (for review see Bean (2007)). This was not the case. Figure 4a shows the mean waveforms for 50 neurons recorded on each cortical area studied and the average of these means (the height of the waveforms was normalized to aid in comparing spike widths). Surprisingly, waveforms from the FAF and AC had similar shapes and durations. To quantify the shape of the spikes, we calculated the area under the absolute value of the average spike waveform for each unit studied. The area under waveform distributions

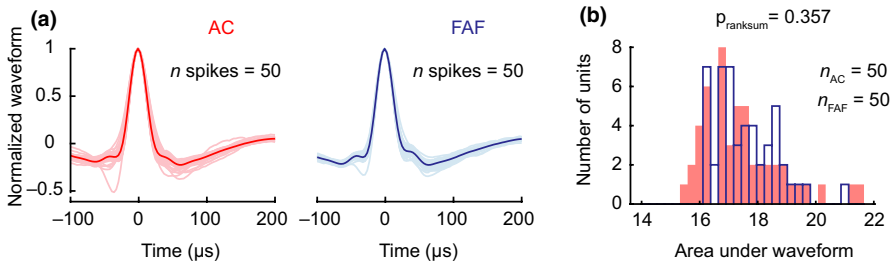

FIGURE 4 No differences in spike waveforms between units from auditory cortex (AC) and frontal auditory field (FAF). (a) Average waveforms of each of the 50 units recorded in the AC (left) and in the FAF (right). The thicker line indicates the mean of the averages. (b) Distributions of mean areas under the absolute value of the spike waveform obtained in each location (AC and FAF). [Colour figure can be viewed at wileyonlinelibrary.com]

(Figure 4b) did not differ statistically between the AC and FAF (Wilcoxon rank-sum test, p-value = 0.357). The latter suggests that similar current dynamics are involved in spike generation in these two structures.

3.2 | Subthreshold, long-lasting excitation could explain FAF response properties

Our electrophysiological data showed that FAF neuronal properties differ strongly from those found in the AC. In comparison with AC neurons, FAF neurons have slower spiking (in terms of ISI) and longer-lasting responses, which are loosely time-locked to auditory stimuli. It is unknown which mechanisms shape the firing properties of FAF neurons, causing responses in this structure to differ from those found in the AC (this last structure provides afferent information to the FAF). To address this issue, we created a simple leaky integrate-and-fire neuron model of an FAF neuron. The cellular properties of our model neuron (see Methods Equation (1)) are specified by seven parameters. We constrained the parameters by comparing the simulated responses of the FAF model neurons to the experimental data.

We modelled the input to the FAF neuron model (i.e., the response of AC projections driving FAF neurons) as a Poisson point process mimicking the average spiking of AC

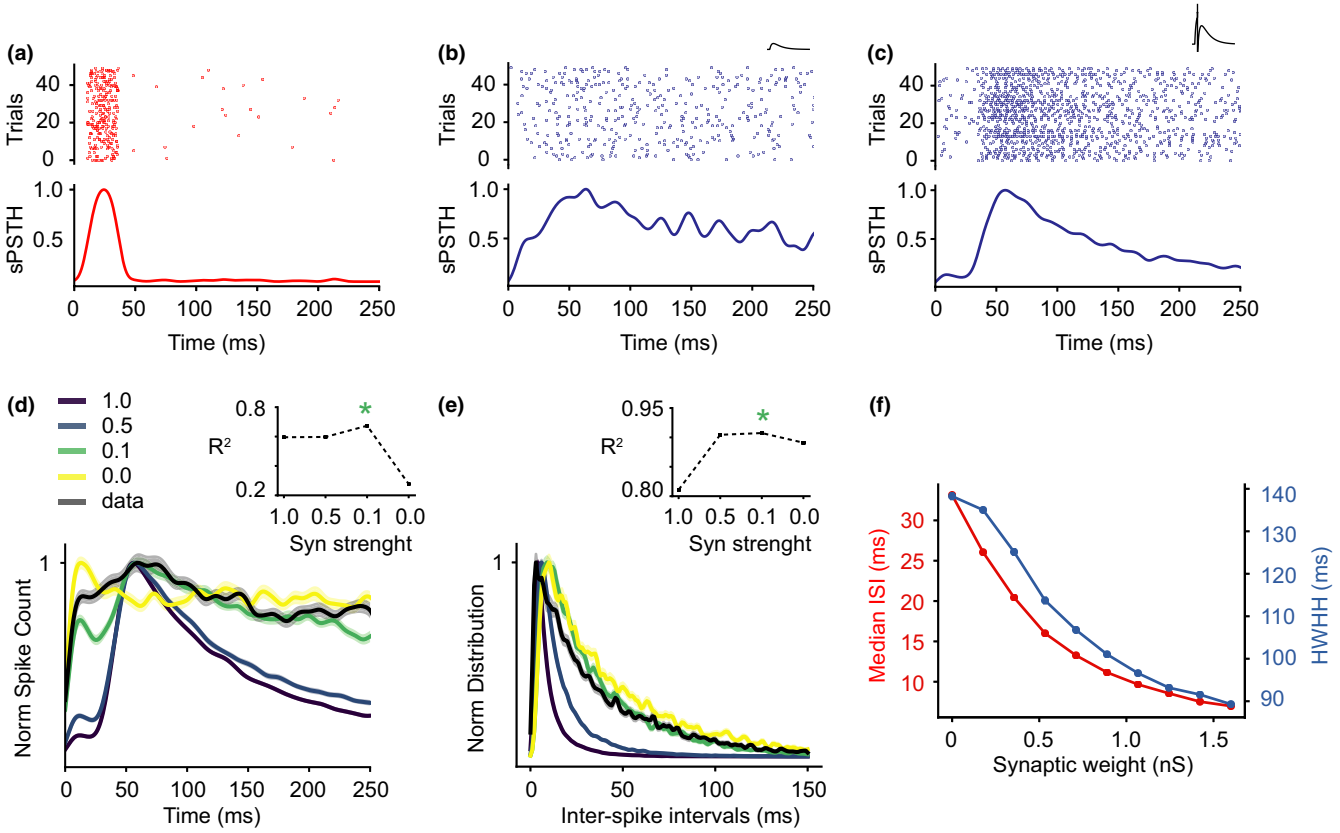

FIGURE 5 A simple model of frontal auditory field (FAF) neuron suggests that subthreshold synaptic excitatory potential could explain the observed spiking pattern. (a) Shows a raster plot generated by a Poisson process mimicking one auditory cortex (AC) neuron response to a pure tone, below the corresponding smooth poststimulus time histograms (sPSTH). (b) Shows the spiking of 50 neuron models in response to the Poissonic input shown in (a). On the top, the raster plot and below, the corresponding sPSTH. The synaptic weight was set to 0.3 nS in order to generate a subthreshold excitatory postsynaptic potential as indicated in the inset. The value used corresponds to a 18% of the minimum suprathreshold synaptic weight (1.6 nS). In (c), the same plots than in (b) are shown, however the synaptic weight in these simulations was set to 1.6 ns. One synapse is able to generate a spike in the neuron model, as indicated in the inset. In (b) and (c) the time constant of the synapse model was set to 90 ms. (d) Shows sPSTH obtained from four simulations using different values of synaptic strength, defined as the ratio between the parameter w_e used and the minimum value of w_e necessary to reach a postsynaptic spike. The synaptic strengths used are shown in the legend. The average sPSTH from real data is plotted in black. The inset shows the Pearson correlation coefficient calculated between each simulated sPSTH and the average sPSTH obtained from all units. The asterisk indicates the higher value. (e) Shows the normalized ISI distributions for the same simulations ran in (d). The inset shows the Pearson correlation coefficient calculated between these curves and the average ISI distribution obtained from all units. The asterisk indicates the higher value. (f) Shows the median of ISI and the half-width half-height (HWHH) of autocorrelogram of sPSTH calculated from 10 simulations in which systematically increasing the strength of the synapse, from 0 to 1.6 nS. Error bars indicate standard errors across 50 simulations. [Colour figure can be viewed at wileyonlinelibrary.com]

neurons. Figure 5a shows the raster plot from a simulation of 50 Poisson processes and the respective event counts below (sPSTH, bin size of 5 ms). Note that both the simulated and the observed AC (Figure 3c) sPSTHs represent transient responses lasting less than 100 ms.

Since we showed that neurons in the AC and FAF exhibit statistically similar spike waveforms (see Figure 4), we assumed that the modifications to input–output features of FAF neurons rely on synaptic properties more than on intrinsic neuronal properties. This assumption was based on several studies that have shown that the spike shape reflects kinetics and distribution of ion channels (Henze et al., 2000; Martina & Jonas, 1997). Therefore, we investigated the effects of the synaptic weight and duration on the spiking of the FAF neuron model.

First, we investigated how the magnitude of the synaptic depolarization changed the firing properties of the FAF neuron model. Our results indicated that the postsynaptic effect must be subthreshold (or near-threshold) to reproduce the FAF data. In our model, a presynaptic spike induces conductance changes according to Equation (2), (3) and (4) (see Methods section), which can produce (or not) a postsynaptic spike depending on the strength of the synapse. According to the parameters set, the minimum suprathreshold synaptic weight of our neuron model is 1.6 nS. Therefore, to generate a subthreshold excitatory postsynaptic potential, the synaptic weight was set at 0.3 nS, which corresponds to 18% of 1.6 nS. In Figure 5b, we plotted the raster and the corresponding sPSTH from 50 FAF simulated neurons (or trials, no difference in our model), in response to the spike trains shown in 5a, when one presynaptic spike generates a small depolarization in the postsynaptic membrane potential as shown in the inset. The obtained sPSTH was qualitatively similar to the one obtained in FAF recordings (see sPSTH in Figure 3c). In contrast, when the modelled AC-FAF synapse was strong enough to produce a postsynaptic spike (synaptic weight = 1.6 nS, see inset in Figure 5c), the simulations rendered an sPSTH with high amplitude response, qualitatively different from those observed in our FAF data. In both simulations (Figure 5b,c), the synaptic time constant was 90 ms (see below).

To systematically examine the effect of the synaptic strength on the shape of the sPSTH obtained from 50 neuron models, we ran four different simulations varying the synaptic weight (Figure 5d) and compared them directly with the average data from all FAF units recorded (black curve). Here, we refer to synaptic strength as the ratio between the synaptic weight (w_e, described in Equation (4) in Methods) and the minimum w_e needed to generate one spike in our FAF neuron model:

$$S_{\text{strength}} = \frac{w_e}{min\ suprath.w_e}$$

We tested synaptic strength values of 0, 0.1, 0.5 and 1. As shown in Figure 5c, simulations with suprathreshold synaptic strengths (synaptic strength = 1) rendered an sPSTH with a short but high amplitude peak in response to the input, qualitatively different from that obtained in the data. When the synaptic strength was decreased to 0.5, FAF simulated responses decreased in amplitude and increased in duration, and however, the sPSTH differed from that obtained from FAF data. When the synaptic strength was set to 0.1, we obtained simulation results that resembled more the FAF data, consistent with a high value of Pearson correlation coefficient ($r = 0.66$) between the simulated sPSTH and the average sPSTH obtained from FAF recordings (indicated with an asterisk in the inset). As expected, when the synaptic strength was set to 0, there was no evoked response and the sPSTH reflected the spontaneous activity implemented in the neuron model.

In the preceding text, we also reported that FAF neurons have slow spiking dynamics (shown in higher values of median ISI when compared to the AC, see Figure 3f). Therefore, for the same four simulations varying the w_e, we calculated the ISI distributions (Figure 5e). For decreasing values of synaptic strength, the ISI distribution shifted to higher time intervals, indicative of slower spiking. Again, setting the synaptic strength to 0.1 led to the highest Pearson correlation coefficient ($r = .91$, indicated with an asterisk in the inset) between the ISI data distribution and the four different simulation distributions.

To summarize these results, in Figure 5f, we ran 10 simulations covering a larger range of subthreshold synaptic strengths and plotted, for each simulation, the median ISI and the HWHH. Both parameters decrease with increasing the synaptic strength, indicating that stronger synapses reduce the differences between input and output spiking. Based on these simulation results, we hypothesize that the increased HWHH and ISI observed in the FAF when compared to the AC could be the result of weak excitability power in AC-FAF projections. Note that with our model we cannot disentangle whether this weak excitability power is the result of weak synapses or low resting membrane potentials in FAF neurons. The latter could result, for example, from inhibitory regimes.

Next, we investigated how the duration of the synaptic depolarization changed the firing of the FAF neuron model. Figure 6a,b shows simulations in which the time course of the synaptic conductance change, given by the parameter τ_e, was set to 10 and 90 ms, respectively. The postsynaptic potentials modelled in each case can be seen in the respective insets. In both simulations, the synaptic strength was subthreshold and fixed to 0.1 (ratio compared to the minimum suprathreshold conductance, see preceding text). The simulated sPSTH showed that shorter excitatory postsynaptic potentials (Figure 6a) result in shorter responses

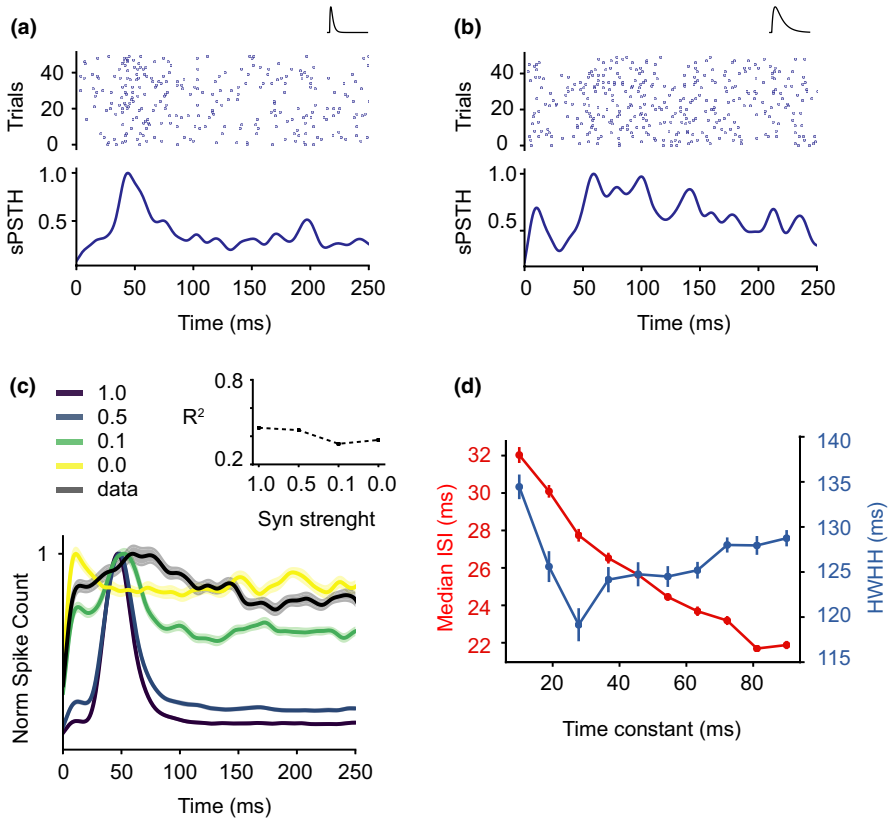

FIGURE 6 A simple model of frontal auditory field (FAF) neuron suggests that long-lasting synapse is also needed to explain the observed spiking pattern. (a) and (b) Show simulations in response to the spikes showed in Figure 4a, with different postsynaptic durations. On top, the raster plot and below, the respective smooth poststimulus time histograms (sPSTH). In (a), the time constant of the synaptic conductance change was set to 10 ms, the change in the membrane potential produced by one presynaptic spike is showed in the inset. In (b), the time constant was set to 90 ms. Note that the excitatory postsynaptic potential in the inset is longer in comparison with the inset in (a). In (a) and (b), the synaptic weight was set to 4.3 and 0.3 nS, respectively. Both values correspond to a 18% of the minimum suprathreshold synaptic weight of each model. (c) Shows the sPSTHs obtained from four simulations changing the synaptic strength as showed in Figure 4d. The synaptic strengths used are shown in the legend. In these simulations, we set a shorter synaptic time constant than that in Figure 4d (τ_e = 10 ms instead of 90 ms). The average sPSTH from real data is plotted in black. Note that even with the lowest synaptic strength tested (ratio = 0.1), the Pearson correlation coefficient (showed in the inset) is lower than those obtained in Figure 4d, using longer synaptic time constant. (d) The median of ISI and half-width half-height (HWHH) of autocorrelograms of sPSTHs obtained from 10 simulations in which the duration of the postsynaptic effect was systematically increased, by changing τ_e from 10 to 90 ms. Error bars indicate standard error across 50 simulations. [Colour figure can be viewed at wileyonlinelibrary.com]

that those obtained using longer time constants (Figure 6b). Note that simulations with longer excitatory postsynaptic potentials reproduced more closely the sPSTHs observed experimentally (see Figure 3c).

To make sure that long synaptic conductance was indeed needed to reproduce experimental data, we ran the same simulations as in Figure 5c; however, in this case, the synaptic time constant was set to 10 ms (it was 90 ms in Figure 5c). None of the simulations obtained using 10-ms time constant were able to better reproduce qualitatively the experimental data (showed in black), consistent with lower values of Pearson correlation coefficients (r_{max} = 0.45) in relation to those obtained with 90-ms time constant (compare with inset Figure 5d). These *R* values (inset Figure 6c) were calculated by correlating the average data and the four different simulated sPSTHs. Overall, the simulation results indicate that low synaptic strength is not enough to reproduce FAF responses. Long excitatory postsynaptic potentials are also needed.

Finally, we ran 10 simulations in which the synaptic time constant was systematically increased from 10 to 90 ms. For each simulation, the median ISI and the HWHH from the neuron model output was analysed (Figure 6d). The median ISI decreases with increasing time constant, indicating that longer excitatory postsynaptic potentials enable an increment in the rate of temporal summation, and consequently, the probability of spike occurrence increases. On the other hand, HWHHs changed in a complex U-shaped manner with increasing time constants. Note that the experimental data on FAF responses showed high ISI and HWHH values (Figure 3). Based on our simulations, high ISI-HWHH combinations can be achieved only with long synaptic time constants.

4 | DISCUSSION

The main aim of this article was to compare response properties of auditory neurons found in the bat FAF and AC regions. We used identical recording and stimulation settings for studying these two structures in order to assess modifications to neuronal responses in the AC-FAF pathway. Our results show that FAF neurons are responsive to sounds, and however, when compared to auditory cortex neurons, they presented sparser, less precise spiking and longer-lasting responses to pure tones. Based on results from a leaky integrate-and-fire neuronal model, we speculate that slow, weak synaptic dynamic could contribute to the changes in activity pattern that occur as information travels through cortico-cortical projections from the AC to the FAF.

4.1 | Possible origin and function of FAF responses

We found that, in general, peak response latencies to auditory stimuli are longer in FAF than in AC neurons. These latency differences suggest that cortical feedforward projections evoke responses in the FAF. The latter falls in line with anatomical data showing that the FAF receives cortical afferents (Kobler et al., 1987). However, this does not mean that AC inputs are the only source for driving FAF spiking. FAF neurons also receive afferents from auditory structures that bypass the AC, such as the suprageniculate nucleus of the thalamus (Kobler et al., 1987). To our knowledge, detailed anatomical and electrophysiological data of suprageniculate afferents to the FAF are presently not available. How different inputs sources to the FAF (e.g., suprageniculate and cortical) interact at the single neuron level remains obscure. One could speculate that non-cortical inputs travelling through the suprageniculate nucleus could arrive to the FAF before cortical inputs. In our data, we did observe a small subpopulation of FAF neurons that had peak latencies shorter than 20 ms (10% of the recorded units, see Figure 3d), although these neurons are not predominant. Similar results were described in previous studies on frontal responses in bats (Eiermann & Esser, 2000; Kanwal et al., 2000). Note that with our data, we cannot disentangle whether neurons with fast latencies in the FAF result from fast projections from the AC or from fast afferents travelling through the suprageniculate nucleus.

Another possibility that requires consideration is that fast suprageniculate inputs could change the *status quo* in FAF neurons by controlling their membrane potential. Because most FAF neurons have long peak latencies, it is likely that suprageniculate afferents alone are not capable of evoking FAF spiking. The latter could occur either because suprageniculate inputs are excitatory but not strong enough for causing suprathreshold depolarizations or because they are inhibitory. The inhibitory hypothesis is particularly appealing, as it could provide a likely explanation for achieving low FAF excitability which, according to our computational model, is a fundamental requisite for explaining FAF firing properties (see Figure 5). In other species, GABAergic (inhibitory) projections from the Raphe nuclei and basal forebrain to frontal regions have been described (Carr & Sesack, 2000; Henny & Jones, 2008). In addition, inhibition via interneurons could also decrease FAF excitability.

Our data show higher spiking variability (i.e., inter-trial variability calculated as Jaccard coefficients) in frontal neurons when compared to AC neurons (see individual examples in Figure 2c,d and population data in Figure 3h). This result is consistent with previous studies in bats and primates describing neuronal responses to auditory stimuli in frontal areas as irregular and variable (Eiermann & Esser, 2000; Kanwal et al., 2000; Newman & Lindsley, 1976). Even though neural activity across sensory pathways increases in variability (Vogel, Hennig, & Ronacher, 2005), studies indicate that this "variability" or output "noise" might offer processing advantages. Noisy responses could result from large excitability fluctuations in the neurons studied which could make these neurons more prone to control through processes such as attention or multi-sensory integration. In other animal species, these processes are known to influence frontal responses (Tomita, Ohbayashi, Nakahara, Hasegawa, & Miyashita, 1999; Watanabe, 1992) and they could also do so in bats. Interestingly, studies have suggested that intrinsic noise could enhance sensitivity to weak signals (Stein, Gossen, & Jones, 2005). The latter might be important for bats that have to cope with faint signals during navigation (i.e., echoes) often in noisy environments (Corcoran & Moss, 2017).

Other authors have discussed a possible role of the FAF in novelty detection and sensorimotor integration (Eiermann & Esser, 2000; Kanwal et al., 2000). The FAF could participate in the integration of sensory inputs over time and coordinate motor acts (as pinna movements, mimic reactions and vocalizations) in response to sensory information. We speculate that the strength of feedforward inputs reaching the FAF could dynamically change with the behavioural context. Weak feedforward inputs (as those predicted by our model) could be particularly susceptible to modifications through processes such as attention, learning and multi-sensory integration. The existence of FAF subregions with different functions remains unknown. In our data, we observed that ~10% of the FAF neurons recorded had latencies <20 ms (Figure 3d). This subpopulation of neurons deviates from the average response properties found in the FAF (average latency ~90 ms, see Figure 3c). Future experiments, with an anatomical focus, are required to assess possible correlations between physiological properties (as response latency) and anatomical location in the bat frontal cortex.

It has been argued that response variability might be overestimated simply because we do not understand what high-order neurons are signalling (Masquelier, 2013). This could explain why responses from frontal neurons are less reliable than those of cortical neurons when tested with simple stimuli such as the pure tones used in this study. The reliability of neuronal responses could increase during active behaviour (i.e., echolocation), which involves a set of variables such as attention, and the build-up of expectations based on previous sensory history (Feng & Ratnam, 2000; Wohlgemuth, Kothari, & Moss, 2016). The roles of these variables are much diminished in experiments conducted in anaesthetized, passively listening animals (this study). Nevertheless, the responses observed in our study are largely similar to those reported in previous work done in awake bats (Eiermann & Esser, 2000). Future studies should investigate neuronal responses in awake animals during active behaviour, to better understand auditory processing in frontal areas. In any case, it should be considered that experiments conducted under anaesthesia could give insight into intrinsic properties of the neurons studied and disregarding how these properties might be influenced by complex phenomena such as attention.

Both experimental conditions mentioned above are as follows: simple stimuli and the use of anaesthesia during recordings constitute limitations of the present study, particularly when considering that the FAF participates in a cognitive control on sensory processing. In rats, the amygdala is connected to the frontal cortex (Swanson & Petrovich, 1998) and it is important in aversive and rewarding experiences (Davis & Whalen, 2001), as well as in mediating social interactions. It has been shown that the basolateral amygdala in the bat brain responds strongly to social calls (Gadziola, Shanbhag, & Wenstrup, 2016; Naumann & Kanwal, 2011). Consequently, using naturalistic stimuli could increase the strength of possible amygdala-triggered FAF responses and, therefore, when using natural stimuli FAF response characteristics might differ from those reported here. At presently, it is unclear how amygdala responses modulate FAF activity (and vice versa). Future studies recording simultaneously from these two areas could shed light into this issue. In addition, it has been shown that frontal cortex neurons in ferrets are behaviourally gated and highly selective for target stimuli (Fritz, David, Radtke-Schuller, Yin, & Shamma, 2010). During goal-directed behaviours, it is expected that task-dependent inputs modify activity in frontal neurons. These effects are not accessible under our experimental conditions.

4.2 | FAF response properties could be linked to the strength of afferent projections

To our knowledge, at present, histochemical, anatomical and biophysical data regarding the bat FAF are very limited. We implemented a simple leaky integrate-and-fire neuronal model to gain insights into the cellular mechanisms that could explain the nature of FAF responses. Similar models have been widely used in neurophysiological studies for understanding sensory processing (Kremer, Leger, Goodman, Brette, & Bourdieu, 2011; Rossant, Leijon, Magnusson, & Brette, 2011). Our aim with this model was to show, in the simplest configuration imaginable, how it is possible to achieve neuronal responses as those recorded in the bat FAF considering only AC feedforward inputs and their properties. Based on our empirical data, the FAF displays slow, irregular, long-lasting responses, while AC spiking is reliable and temporally precise (see Figure 3). Note that our model was based only on AC afferents. Extralemniscal inputs travelling through the suprageniculate nucleus could be even more reliable and precise than AC afferents (see preceding text).

It has been shown that FM-FM stimuli are more effective drivers than single FMs or tones in the majority FAF neurons (Eiermann & Esser, 2000). It is possible that this neuronal preference to FM pairs is consequence of AC inputs properties. Even the AC inherit this property from lower structures in the auditory pathway (Hechavarria & Kossl, 2014). In this study, we did not test responses to FM pairs. However, in principle, our model could render a form of preference to temporally delayed sound pairs due to temporal summation.

Even though our model is very reductionist (e.g., it does not consider either inhibitory inputs nor possible interactions within the FAF), it still was capable of recreating basic properties of FAF neural activity based solely on long, weak excitatory postsynaptic potentials (see Figures 5 and 6). Both synaptic features suggest mechanisms by which FAF neurons can integrate different auditory activity over long periods of time by temporal or spatial summation of presynaptic inputs. In our model, we modified the "synaptic strength" to recreate FAF response properties. However, we cannot disentangle whether "synaptic strength" is linked directly to properties of presynaptic or postsynaptic neurons, or both. At the postsynaptic level, low synaptic strength could be caused, for example, by a low number of excitatory receptor channels or by very negative resting membrane potentials linked to inhibitory regimes (Puig, Artigas, & Celada, 2005; Wehr & Zador, 2003). At the presynaptic level, low synaptic strength could be associated with a number of factors that ultimately decrease the amount of neurotransmitter that reaches postsynaptic neurons. In principle, all of the aforementioned mechanisms are plausible and not mutually exclusive ways to achieve low amplitude postsynaptic potentials in FAF neurons.

Our model also indicates that to achieve FAF-like responses, slow depolarizations are needed (see Figure 6). AMPA and NMDA receptors are the primary mediators of excitatory synaptic transmission in the cortex (Ozawa, Kamiya, & Tsuzuki, 1998). It is known that NMDA receptor

channels show slower kinetics than AMPA receptor channels (Sanchez, Gans, & Wenstrup, 2007). We therefore suggest that NMDA receptors play a major role in mediating postsynaptic responses in FAF neurons. Future studies using pharmacological tools could test this prediction.

Overall, the results presented in this manuscript indicate that the neural codes for sensory information representation change as signal travels from sensory to more complex association cortex areas located in the frontal cortex. A simple way to achieve these response transformations could be linked to the dynamics of feedforward synaptic activity in charge of driving spiking in frontal cortices.

ACKNOWLEDGEMENTS

We are thankful to Manfred Kössl for his insightful comments and to the German Research Foundation (Deutsche Forschungsgemeinschaft, DFG, Project number 275755787).

CONFLICT OF INTEREST

No conflict of interest is declared by the authors.

DATA AVAILABILITY STATEMENT

The data that support the findings of this study are available from the corresponding authors upon reasonable request.

ORCID

Luciana López-Jury https://orcid.org/0000-0002-9384-2586
Francisco García-Rosales https://orcid.org/0000-0001-5576-2967
Julio C. Hechavarria https://orcid.org/0000-0001-9277-2339

REFERENCES

Azuma, M., & Suzuki, H. (1984). Properties and distribution of auditory neurons in the dorsolateral prefrontal cortex of the alert monkey. *Brain Research*, *298*, 343–346. https://doi.org/10.1016/0006-8993(84)91434-3

Bean, B. P. (2007). The action potential in mammalian central neurons. *Nature Reviews Neuroscience*, *8*, 451–465. https://doi.org/10.1038/nrn2148

Carmichael, S. T., & Price, J. L. (1995). Sensory and premotor connections of the orbital and medial prefrontal cortex of macaque monkeys. *The Journal of Comparative Neurology*, *363*, 642–664. https://doi.org/10.1002/cne.903630409

Carr, D. B., & Sesack, S. R. (2000). GABA-containing neurons in the rat ventral tegmental area project to the prefrontal cortex. *Synapse (New York, N. Y.)*, *38*, 114–123. https://doi.org/10.1002/1098-2396(20001)38:2<114:AID-SYN2>3.0.CO;2-R

Casseday, J. H., Kobler, J. B., Isbey, S. F., & Covey, E. (1989). Central acoustic tract in an echolocating bat: An extralemniscal auditory pathway to the thalamus. *The Journal of Comparative Neurology*, *287*, 247–259. https://doi.org/10.1002/cne.902870208

Constantinidis, C., & Goldman-Rakic, P. S. (2002). Correlated discharges among putative pyramidal neurons and interneurons in the primate prefrontal cortex. *Journal of Neurophysiology*, *88*, 3487–3497. https://doi.org/10.1152/jn.00188.2002

Corcoran, A. J., & Moss, C. F. (2017). Sensing in a noisy world: Lessons from auditory specialists, echolocating bats. *Journal of Experimental Biology*, *220*, 4554–4566. https://doi.org/10.1242/jeb.163063

Davis, M., & Whalen, P. J. (2001). The amygdala: Vigilance and emotion. *Molecular Psychiatry*, *6*, 13–34. https://doi.org/10.1038/sj.mp.4000812

Eiermann, A., & Esser, K. H. (2000). Auditory responses from the frontal cortex in the short-tailed fruit bat *Carollia perspicillata*. *NeuroReport*, *11*, 421–425. https://doi.org/10.1097/00001756-200002070-00040

Esser, K.-H. (2003). Modeling aspects of speech processing in bats—Behavioral and neurophysiological studies. *Speech Communication*, *41*, 179–188. https://doi.org/10.1016/S0167-6393(02)00102-4

Esser, K. H., & Eiermann, A. (1999). Tonotopic organization and parcellation of auditory cortex in the FM-bat *Carollia perspicillata*. *European Journal of Neuroscience*, *11*, 3669–3682. https://doi.org/10.1046/j.1460-9568.1999.00789.x

Feng, A. S., & Ratnam, R. (2000). Neural basis of hearing in real-world situations. *Annual Review of Psychology*, *51*, 699–725. https://doi.org/10.1146/annurev.psych.51.1.699

Fritz, J. B., David, S. V., Radtke-Schuller, S., Yin, P. B., & Shamma, S. A. (2010). Adaptive, behaviorally gated, persistent encoding of task-relevant auditory information in ferret frontal cortex. *Nature Neuroscience*, *13*, 1011–1019. https://doi.org/10.1038/nn.2598

Fuster, J. M. (2000). Prefrontal neurons in networks of executive memory. *Brain Research Bulletin*, *52*, 331–336. https://doi.org/10.1016/S0361-9230(99)00258-0

Fuster, J. M. (2001). The prefrontal cortex–an update: Time is of the essence. *Neuron*, *30*, 319–333. https://doi.org/10.1016/S0896-6273(01)00285-9

Gadziola, M. A., Shanbhag, S. J., & Wenstrup, J. J. (2016). Two distinct representations of social vocalizations in the basolateral amygdala. *Journal of Neurophysiology*, *115*, 868–886. https://doi.org/10.1152/jn.00953.2015

Garcia-Rosales, F., Beetz, M. J., Cabral-Calderin, Y., Kossl, M., & Hechavarria, J. C. (2018). Neuronal coding of multiscale temporal features in communication sequences within the bat auditory cortex. *Communications Biology*, *1*, 200. https://doi.org/10.1038/s42003-018-0205-5

Goldman-Rakic, P. S. (1995). Architecture of the prefrontal cortex and the central executive. *Annals of the New York Academy of Sciences*, *769*, 71–83. https://doi.org/10.1111/j.1749-6632.1995.tb38132.x

Goldman-Rakic, P. S., & Porrino, L. J. (1985). The primate mediodorsal (MD) nucleus and its projection to the frontal lobe. *The Journal of Comparative Neurology*, *242*, 535–560. https://doi.org/10.1002/cne.902420406

Goodman, D. F., & Brette, R. (2009). The Brian simulator. *Frontiers in Neuroscience*, *3*(2), 192–197. https://doi.org/10.3389/neuro.01.026.2009

Hackett, T. A., Stepniewska, I., & Kaas, J. H. (1999). Prefrontal connections of the parabelt auditory cortex in macaque

monkeys. *Brain Research*, *817*, 45–58. https://doi.org/10.1016/S0006-8993(98)01182-2

Hagemann, C., Esser, K. H., & Kossl, M. (2010). Chronotopically organized target-distance map in the auditory cortex of the short-tailed fruit bat. *Journal of Neurophysiology*, *103*, 322–333. https://doi.org/10.1152/jn.00595.2009

Hechavarria, J. C., & Kossl, M. (2014). Footprints of inhibition in the response of cortical delay-tuned neurons of bats. *Journal of Neurophysiology*, *111*, 1703–1716. https://doi.org/10.1152/jn.00777.2013

Henny, P., & Jones, B. E. (2008). Projections from basal forebrain to prefrontal cortex comprise cholinergic, GABAergic and glutamatergic inputs to pyramidal cells or interneurons. *European Journal of Neuroscience*, *27*, 654–670. https://doi.org/10.1111/j.1460-9568.2008.06029.x

Henze, D. A., Borhegyi, Z., Csicsvari, J., Mamiya, A., Harris, K. D., & Buzsaki, G. (2000). Intracellular features predicted by extracellular recordings in the hippocampus in vivo. *Journal of Neurophysiology*, *84*, 390–400. https://doi.org/10.1152/jn.2000.84.1.390

Ito, T., Yamamoto, R., Furuyama, T., Hase, K., Kobayasi, K. I., Hiryu, S., & Honma, S. (2019). Three forebrain structures directly inform the auditory midbrain of echolocating bats. *Neuroscience Letters*, *712*, 134481. https://doi.org/10.1016/j.neulet.2019.134481

Kanwal, J. S., Fitzpatrick, D. C., & Suga, N. (1999). Facilitatory and inhibitory frequency tuning of combination-sensitive neurons in the primary auditory cortex of mustached bats. *Journal of Neurophysiology*, *82*, 2327–2345. https://doi.org/10.1152/jn.1999.82.5.2327

Kanwal, J. S., Gordon, M., Peng, J. P., & Heinz-Esser, K. (2000). Auditory responses from the frontal cortex in the mustached bat, *Pteronotus parnellii*. *NeuroReport*, *11*, 367–372. https://doi.org/10.1097/00001756-200002070-00029

Kanwal, J. S., & Rauschecker, J. P. (2007). Auditory cortex of bats and primates: Managing species-specific calls for social communication. *Frontiers in Bioscience*, *12*, 4621–4640. https://doi.org/10.2741/2413

Kayser, C., Logothetis, N. K., & Panzeri, S. (2010). Millisecond encoding precision of auditory cortex neurons. *Proceedings of the National Academy of Sciences of the United States of America*, *107*, 16976–16981. https://doi.org/10.1073/pnas.1012656107

Kobler, J. B., Isbey, S. F., & Casseday, J. H. (1987). Auditory pathways to the frontal cortex of the mustache bat, *Pteronotus parnellii*. *Science*, *236*, 824–826. https://doi.org/10.1126/science.2437655

Kremer, Y., Leger, J. F., Goodman, D., Brette, R., & Bourdieu, L. (2011). Late emergence of the vibrissa direction selectivity map in the rat barrel cortex. *Journal of Neuroscience*, *31*, 10689–10700. https://doi.org/10.1523/JNEUROSCI.6541-10.2011

Macias, S., Hechavarria, J. C., & Kossl, M. (2016). Temporal encoding precision of bat auditory neurons tuned to target distance deteriorates on the way to the cortex. *Journal of Comparative Physiology A*, *202*, 195–202. https://doi.org/10.1007/s00359-016-1067-2

Martina, M., & Jonas, P. (1997). Functional differences in Na+ channel gating between fast-spiking interneurones and principal neurones of rat hippocampus. *Journal of Physiology*, *505*(Pt 3), 593–603.

Masquelier, T. (2013). Neural variability, or lack thereof. *Frontiers in Computational Neuroscience*, *7*, 7. https://doi.org/10.3389/fncom.2013.00007

Naumann, R. T., & Kanwal, J. S. (2011). Basolateral amygdala responds robustly to social calls: Spiking characteristics of single unit activity. *Journal of Neurophysiology*, *105*, 2389–2404. https://doi.org/10.1152/jn.00580.2010

Newman, J. D., & Lindsley, D. F. (1976). Single unit analysis of auditory processing in squirrel monkey frontal cortex. *Experimental Brain Research*, *25*, 169–181. https://doi.org/10.1007/BF00234901

Ozawa, S., Kamiya, H., & Tsuzuki, K. (1998). Glutamate receptors in the mammalian central nervous system. *Progress in Neurobiology*, *54*, 581–618. https://doi.org/10.1016/S0301-0082(97)00085-3

Plakke, B., Ng, C. W., & Poremba, A. (2013). Neural correlates of auditory recognition memory in primate lateral prefrontal cortex. *Neuroscience*, *244*, 62–76. https://doi.org/10.1016/j.neuroscience.2013.04.002

Plakke, B., & Romanski, L. M. (2014). Auditory connections and functions of prefrontal cortex. *Frontiers in Neuroscience*, *8*, 199. https://doi.org/10.3389/fnins.2014.00199

Puig, M. V., Artigas, F., & Celada, P. (2005). Modulation of the activity of pyramidal neurons in rat prefrontal cortex by raphe stimulation in vivo: Involvement of serotonin and GABA. *Cerebral Cortex*, *15*, 1–14. https://doi.org/10.1093/cercor/bhh104

Rao, S. C., Rainer, G., & Miller, E. K. (1997). Integration of what and where in the primate prefrontal cortex. *Science*, *276*, 821–824. https://doi.org/10.1126/science.276.5313.821

Romanski, L. M., Bates, J. F., & Goldman-Rakic, P. S. (1999). Auditory belt and parabelt projections to the prefrontal cortex in the rhesus monkey. *The Journal of Comparative Neurology*, *403*, 141–157. https://doi.org/10.1002/(SICI)1096-9861(19990111)403:2<141:AID-CNE1>3.0.CO;2-V

Romanski, L. M., Tian, B., Fritz, J., Mishkin, M., Goldman-Rakic, P. S., & Rauschecker, J. P. (1999). Dual streams of auditory afferents target multiple domains in the primate prefrontal cortex. *Nature Neuroscience*, *2*, 1131–1136. https://doi.org/10.1038/16056

Rossant, C., Leijon, S., Magnusson, A. K., & Brette, R. (2011). Sensitivity of noisy neurons to coincident inputs. *Journal of Neuroscience*, *31*, 17193–17206. https://doi.org/10.1523/JNEUROSCI.2482-11.2011

Sanchez, J. T., Gans, D., & Wenstrup, J. J. (2007). Contribution of NMDA and AMPA receptors to temporal patterning of auditory responses in the inferior colliculus. *Journal of Neuroscience*, *27*, 1954–1963. https://doi.org/10.1523/JNEUROSCI.2894-06.2007

Stein, R. B., Gossen, E. R., & Jones, K. E. (2005). Neuronal variability: Noise or part of the signal? *Nature Reviews Neuroscience*, *6*, 389–397. https://doi.org/10.1038/nrn1668

Swanson, L. W., & Petrovich, G. D. (1998). What is the amygdala? *Trends in Neurosciences*, *21*, 323–331. https://doi.org/10.1016/S0166-2236(98)01265-X

Tomita, H., Ohbayashi, M., Nakahara, K., Hasegawa, I., & Miyashita, Y. (1999). Top-down signal from prefrontal cortex in executive control of memory retrieval. *Nature*, *401*, 699–703. https://doi.org/10.1038/44372

Uylings, H. B., Groenewegen, H. J., & Kolb, B. (2003). Do rats have a prefrontal cortex? *Behavioral Brain Research*, *146*, 3–17. https://doi.org/10.1016/j.bbr.2003.09.028

Vogel, A., Hennig, R. M., & Ronacher, B. (2005). Increase of neuronal response variability at higher processing levels as revealed by simultaneous recordings. *Journal of Neurophysiology*, *93*, 3548–3559. https://doi.org/10.1152/jn.01288.2004

Watanabe, M. (1992). Frontal units of the monkey coding the associative significance of visual and auditory stimuli. *Experimental Brain Research*, *89*, 233–247. https://doi.org/10.1007/BF00228241

Wehr, M., & Zador, A. M. (2003). Balanced inhibition underlies tuning and sharpens spike timing in auditory cortex. *Nature*, *426*, 442–446. https://doi.org/10.1038/nature02116

Wilson, F. A. W., Scalaidhe, S. P. O., & Goldmanrakic, P. S. (1994). Functional synergism between putative gamma-aminobutyrate-containing neurons and pyramidal neurons in prefrontal cortex. *Proceedings of the National Academy of Sciences of the United States of America*, *91*, 4009–4013. https://doi.org/10.1073/pnas.91.9.4009

Wise, S. P. (2008). Forward frontal fields: Phylogeny and fundamental function. *Trends in Neurosciences*, *31*, 599–608. https://doi.org/10.1016/j.tins.2008.08.008

Wohlgemuth, M. J., Kothari, N. B., & Moss, C. F. (2016). Action enhances acoustic cues for 3-D target localization by echolocating bats. *PLoS Biology*, *14*, e1002544. https://doi.org/10.1371/journal.pbio.1002544

SUPPORTING INFORMATION

Additional supporting information may be found online in the Supporting Information section.

How to cite this article: López-Jury L, Mannel A, García-Rosales F, Hechavarria JC. Modified synaptic dynamics predict neural activity patterns in an auditory field within the frontal cortex. *Eur J Neurosci*. 2020;51:1011–1025. https://doi.org/10.1111/ejn.14600